International Journal of Mechanical Sciences 55 (2012) 104–117

Contents lists available at SciVerse ScienceDirect

International Journal of Mechanical Sciences

journal homepage: www.elsevier.com/locate/ijmecsci

Classical and refined shell models for the analysis of nano-reinforced structures

S. Brischetto *, E. Carrera

Department of Mechanical and Aerospace Engineering, Politecnico di Torino, Corso Duca degli Abruzzi 24, 10129 Torino, Italy

ARTICLE INFO

Article history:
Received 7 December 2010
Received in revised form
17 October 2011
Accepted 3 January 2012
Available online 10 January 2012

Keywords:
Shells
Classical two-dimensional theories
Layer wise models
Carbon nanotubes
Clays
Nanocomposites

ABSTRACT

The use of nanocomposites could be an interesting innovation in aeronautics and space structures such as multilayered plates and shells. The static analysis of layered shells embedding nanocomposites is here accomplished by means of classical and refined two-dimensional models. The shells analyzed are simply supported with a sinusoidal pressure applied at the top. These boundary and loading conditions allow the governing equations to be solved in a closed form. In nanocomposites a small amount of nanoscale reinforcements is embedded which have effects on the macroscale properties. The reinforcements considered are carbon nanotubes (CNTs) and clays, the former ones are nanometer-diameter cylinders, the second fillers are nanometer-thin platelets. Several types of nanocomposites are used in the static analysis of the shells proposed, their elastic properties have been obtained from a critical literature review. Classical two-dimensional models such as Classical Lamination Theory (CLT) and First order Shear Deformation Theory (FSDT), and a refined mixed model based on Carrera Unified Formulation (CUF) are used to investigate four shell configurations: a single layered cylindrical shell panel with CNT reinforcements in elastomeric or thermoplastic polymers, a single layered shell with CNT reinforcements in a polymeric matrix embedding carbon fibers, a sandwich shell with external skins in aluminium alloy and an internal core in silicon foam filled with CNTs and a single layered shell with clay reinforcements in a polymeric matrix. The aims of the paper are to demonstrate that the use of classical shell theories is inadequate to investigate the static response of nanocomposite shells, to quantify the beneficial effect of the nanoreinforcements in terms of displacements and stresses, to show that the curvature of shells does not give further effects with respect to the plate case.

1. Introduction

Nanoreinforced materials have important physical, chemical and electromechanical properties [1], these excellent properties propose them as candidates for high-technological engineering applications, in particular in aerospace and biomedical fields. The nanocomposite properties can be modified by changing the volume fraction, shape, and size of the filler particles [2]. Nanocomposites are multiphase materials where at least one constituent phase has one dimension less than 100 nm. The main critical points in the development of nanocomposites are production of nanoreinforcements and control over distribution in size and their dispersions, tailoring interfaces at nanoscale between the constituents and understanding physical phenomena such as stress transfer and fracture. In particular, interfaces have an important role in enhancing the mechanical properties of nanocomposites, if compared with conventional composites or bulk materials [3]. As discussed in Manocha et al. [3] and in Das and Ansari [4], nanoscale reinforcements can be classified as: fibers or tubes with a diameter smaller than 100 nm and an aspect ratio larger than 100 (e.g., carbon nanotubes (CNTs)), plate-like nanofillers where the layered materials have a thickness of the order of 1 nm and an aspect ratio in the other two dimensions of at least 25 (e.g., clays) and three dimensional nanofillers such as nanospheres and nanopowders. The analyses performed in the present paper only consider layered shells embedding nanocomposite materials with CNTs and clays as fillers. CNTs are carbon allotropes with a cylindrical nanostructure discovered by Ijima [5] in 1991. Clays [6] are usually nanolayers fully dispersed in a polymer matrix which give a significant improvement in mechanical strength, thermal stability and barrier properties.

The present paper gives an exhaustive static analysis of simply supported nanocomposite shells subjected to a transverse sinusoidal load at the top. The aims of the paper are to highlight the importance of advanced two-dimensional shell models for the static response of nanocomposite shells discussing the main limitations of classical shell theories, to quantify the improvements of the nanoreinforcements and to point out possible

* Corresponding author. Tel.: +39 011 090 6813; fax: +39 011 090 6899.
E-mail address: salvatore.brischetto@polito.it (S. Brischetto).

0020-7403/$ - see front matter © 2012 Elsevier Ltd. All rights reserved.
doi:10.1016/j.ijmecsci.2012.01.004

curvature effects in shell geometries (see the plate analysis in [7] for comparison purposes). An advanced mixed model and two classical theories are implemented by means of an in-house academic software called MUL2 [8] (acronym of MULtifield problems for MULtilayered structures). The advanced theories obtained via MUL2 have been extensively validated in the authors' earlier works for one-layered and multilayered isotropic and composite plates and shells [9–13]. However, a preliminary assessment is given to demonstrate that advanced theories give a quasi-3D description of composite shells. After this validation, the software can be used reliably for the static analysis of nanocomposite shells. The nanocomposites employed as materials for the embedded layers in the shell investigated will be discussed in the next section, four shell configurations will be analyzed: one-layered cylindrical shell panel in elastomeric or thermoplastic polymers with CNT reinforcement, the same geometry embedding a layer made of a carbon fiber polymer matrix with CNT reinforcement, a sandwich shell embedding a silicon foam core filled with CNTs between two external skins in aluminum alloy and an one-layered polymer matrix shell with clay reinforcements.

1.1. CNT and clay reinforcements

The use of nano-reinforcements has multiple possibilities, only some of these cases are here considered. The most common nano-reinforcements are Carbon Nano-Tubes (CNTs) due to their high stiffness and strength, as well as their ability to act as conductors. A further possibility in order to obtain nanocomposites is the use of clays. The cases here discussed are the most promising given in the literature, in this section the main critical points will be remarked upon. The first proposed material considers the introduction of CNTs as reinforcements in elastomeric and thermoplastic polymers, the second one outlines the benefits of the introduction of CNTs in a carbon fiber reinforced polymeric matrix, the third case considers a silicon foam filled with CNTs, finally the last example concerns the clay reinforcements in a polymer matrix.

1.1.1. Thermoplastic and elastomeric polymers reinforced with CNTs

Carbon Nano-Tubes (CNTs) have been discovered in Japan by Iijima [5] in 1991. They exhibit superior mechanical properties and they are extremely promising because of their strong, light and high toughness characteristics. Experimental and atomic simulations have confirmed their high Young modulus (greater than 1 TPa). The higher mechanical properties and the low mass density (about 1.75 g/cm^3) allow to consider CNTs as the ideal reinforcement in advanced nanocomposites [14], even though there are a lot of difficulties to manufacturing based CNTs nanocomposites with high performances; as discussed in [15–19] CNTs work well as reinforcements if they are homogeneously dislocated in the matrix and if the load is correctly transferred from the matrix to CNTs. Pantano and Capello [14] have developed a micromechanics model to investigate the effectiveness of the introduction of CNTs in polymeric matrices, this model uses a Representative Volume Element (RVE) for the nanocomposite, a constitutive description for both CNTs and polymeric matrix, an opportune characterization of the connection at the interface between CNTs and the matrix, and opportune boundary conditions for the RVE. The RVE in the space generates a staggered array distribution of CNTs. A Finite Element (FE) model of several RVEs has been created by means of the commercial FE code ABAQUS. A nonlinear structural model simulates CNTs, it allows to consider them as rectilinear or sinusoidal where d is the CNTs diameter, l is the wave length and a is its amplitude (see Fig. 1). Both Single-Walled CNTs (SWCNTs) and Double-Walled CNTs (DWCNTs) (external diameter 1.356 nm and internal diameter of the DWCNT 0.676 nm) have been introduced in polymeric matrices with an average volume fraction $V_f = 3\%$. The polymeric matrix has been considered as an isotropic and linear elastic continuum; a thermoplastic polymer with Young modulus $E = 3.11$ GPa and Poisson ratio $\nu = 0.3$, and an elastomeric polymer with Young modulus $E = 3.11$ MPa and Poisson ratio $\nu = 0.499$ have been analyzed. Further details about the micromechanics model employed and a complete overview of the numerical investigation can be found in [15–19] and[14], respectively. In Table 1 the effect of the CNT reinforcement is evaluated in a thermoplastic polymeric matrix in terms of Young modulus, both the cases of adherence and non-adherence between the CNTs and matrix are investigated, for the two conditions some comparisons between rectilinear and sinusoidal CNTs are proposed. It is clearly indicated how the hypothesis of adherence is fundamental to obtaining an improvement of the Young modulus for the nanocomposite materials, this improvement is not

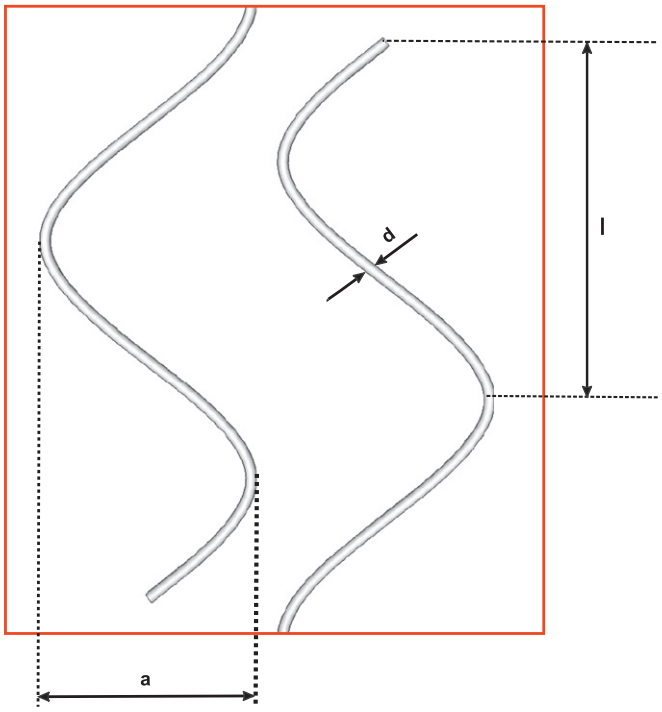

Fig. 1. Geometry of the CNTs embedded in thermoplastic and elastomeric polymers.

Table 1
Thermoplastic polymer (Young modulus $E = 3.11$ GPa and Poisson ratio $\nu = 0.3$) with CNT reinforcement.

CNT geometry	$E_{composite}/E_{polymer}$	$E_{composite}$ (GPa)
No-adherence ($V_f = 3\%$)		
SWCNTs rectilinear	0.996	3.09756
SWCNTs $a/d = 20$, $a/l = 0.173$	0.994	3.09134
DWCNTs $a/d = 20$, $a/l = 0.173$	1.000	3.11000
SWCNTs $a/d = 10$, $a/l = 0.43$	1.039	3.23129
SWCNTs $a/d = 20$, $a/l = 0.43$	1.043	3.24373
DWCNTs $a/d = 20$, $a/l = 0.43$	1.06	3.29660
Adherence ($V_f = 3\%$)		
SWCNTs rectilinear	7.136	22.19296
SWCNTs $a/d = 20$, $a/l = 0.173$	5.23	16.2653
SWCNTs $a/d = 10$, $a/l = 0.43$	3.45	10.7295
SWCNTs $a/d = 20$, $a/l = 0.43$	1.65	5.13150

obtained when the adherence is discarded (for both rectilinear and sinusoidal CNTs). In the case of adherence the nanocomposites with rectilinear CNTs have some advantages for their excellent axial rigidity. It is clear that the inclusion of DWCNTs is more convenient than the use of SWCNTs. This aspect is also verified by some experimental results where the effect of multi-walled CNTs is evaluated in polymeric matrices, the bigger flexional rigidity of multi-walled CNTs is beneficial in such experimental analyses. Pantano and Capello [14] have obtained that the improvements in a nanocomposite with a more rigid matrix, and the same RVE, are less pronounced for the same inclusion of CNTs. This fact is clearly observable in Table 2: when SWCNTs with $a/d=20$, $a/l=0.43$, $V_f=3\%$ and adherence conditions are added in an elastomeric polymer the increase obtained is $E_{composite}/E_{polymer}=12.61$, the improvement is only $E_{composite}/E_{polymer}=1.65$ for the thermoplastic polymer in Table 1 (a more rigid matrix case).

1.1.2. *Polymer matrix embedding carbon fibers reinforced with CNTs*

Carbon Nano-Tubes (CNTs) can also be embedded in a polymer matrix reinforced with carbon fibers. A modified rule of mixture has been employed by Tan et al. [20] to evaluate the elastic properties of such nanocomposites. Delamination is one of the most important problem in laminated fiber reinforced composites because it can significantly reduce the performance of a structure, new composites with through-thickness reinforcement are required to improve the interlaminar strength and damage tolerance of laminated composites [20]. A possible through-thickness reinforcement could be CNTs [21,22], Fig. 2 shows four typical through-thickness reinforcements with nanotube forests. The carbon fiber plane weave composite has rectangular cross-sections of warp and weft yarns and the width and height of the warp yarn are considered to be the same as those for the weft yarn (see Fig. 2). The cases A and B of Fig. 2 have the nanotube forests perpendicular growing to the carbon fiber yarn surfaces, in the cases C and D the nanotube forests vertically grow. The length of nanotubes is considered as a constant and equals 0.01 mm in cases B and D, whereas the nanotube forests grow from the surface of carbon yarn (i.e., warp or weft yarn surface) to the surface of the unit cell in cases A and C. The nanotube forests are assumed to be distributed uniformly and perfectly bonded with the polymer matrix and they are represented by an equivalent continuum tube. The carbon nanotube-reinforced polymer matrices which are obtained by combining the nanotube forests and pure polymer matrix have corresponding mechanical properties which can be obtained by using a modified rule of mixture [20]. Table 3 gives the elastic properties of the three constituents, in Table 4 the effective properties of the four composites shown in Fig. 2 are given by using the analytical approach proposed by Tan et al. [20], the effective properties of the composite without nanotube forests reinforcement are also predicted using the same analytical approach. The chosen nanotube volume fraction for the carbon nanotube-reinforced polymer matrix is 3%. From Table 4 and from the investigation made in [20] about different volume fractions of carbon nanotubes it can be concluded that the effective properties of a composite reinforced with nanotube forests are closely related to the nanotube volume fraction, growing distribution and pattern. The effects of nanotube orientation, out-of-plane Poisson ratios and in-plane shear modulus on the effective properties of the composite reinforced with nanotube forests here discussed are minor. However, the best choice is to separately evaluate each case because the effects of CNTs could be different depending on the chosen material which must be reinforced. The nanotube forests do not significantly affect the in-plane properties of composites. An increase in nanotube volume fraction results in a decrease in the effective out-of-plane Poisson ratios and an increase in the effective out-of-plane Young modulus and shear modulus.

Table 2
Elastomeric polymer (Young modulus $E=3.11$ MPa and Poisson ratio $\nu=0.499$) with CNT reinforcement.

CNT type	$E_{composite}/E_{polymer}$	$E_{composite}$ (MPa)
Adherence ($a/d=20$, $a/l=0.43$)		
SWCNTs ($V_f=1.5\%$)	7.173	22.308
DWCNTs ($V_f=1.5\%$)	8.410	26.154
SWCNTs ($V_f=3.0\%$)	12.61	39.231
DWCNTs ($V_f=3.0\%$)	15.09	46.923
SWCNTs ($V_f=5.0\%$)	20.78	64.615
DWCNTs ($V_f=5.0\%$)	26.71	83.077

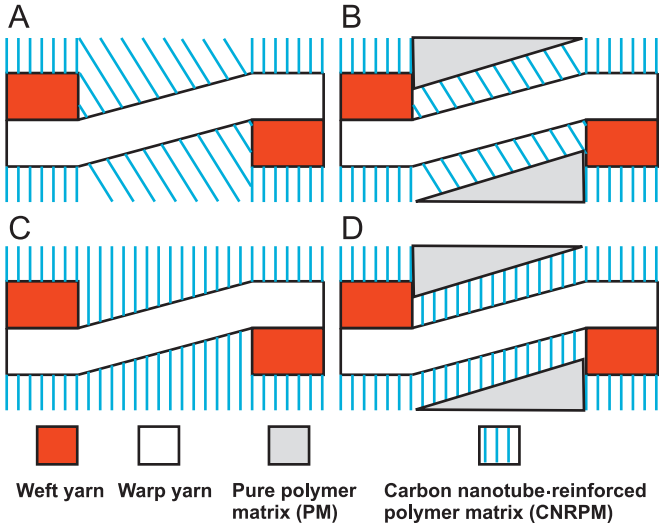

Fig. 2. Typical growing patterns of carbon nanotube forest in a polymer matrix embedding carbon fibers with CNT reinforcement.

Table 3
Elastic properties of the composite constituents of a polymer matrix embedding carbon fibers with CNT reinforcement.

Elastic properties	CNTs	Matrix	Fibers
E_1 (GPa)	1000	3.252	202.038
$E_2=E_3$ (GPa)	600	3.252	12.134
$\nu_{12}=\nu_{13}$	0.19	0.355	0.2128
ν_{23}	0.25	0.355	0.2704
$G_{12}=G_{23}$ (GPa)	500	1.2	8.358
G_{13} (GPa)	500	1.2	4.776

Table 4
Predicted elastic properties of the polymer matrix embedding carbon fibers with and without CNT reinforcement.

Elastic properties	No CNTs	Case A	Case B	Case C	Case D
$E_1=E_2$ (GPa)	69.23	69.34	69.24	69.25	69.35
E_3 (GPa)	9.070	14.61	10.55	14.90	10.56
ν_{12}	0.025	0.025	0.025	0.027	0.026
$\nu_{13}=\nu_{23}$	0.307	0.140	0.260	0.155	0.260
$G_{12}=G_{23}$ (GPa)	4.410	4.415	4.410	4.410	4.410
G_{13} (GPa)	2.840	3.270	2.910	2.880	2.850

1.1.3. Silicon foam reinforced with CNTs

In [23] a foam is reinforced by adding CNTs or functionalized graphene sheets. Free-rising silicon foams were obtained with loading fractions of up to 1.0 wt% carbon nanotubes (CNTs) using hydrogen as a blowing agent. These nanofillers showed a positive effect on the compressive response of the foams. However, the nanocomposite foams had a decrease in the acoustic absorption with nanofiller content, probably due to the variable foam structure and improved stiffness [24,25]. Coleman et al. [24] and Shaffer and Sandler [25] have demonstrated how the addition of carbon nanotubes (CNTs) in polymer matrices can improve their mechanical, electrical and thermal properties; for these reasons, a silicon foam filled with CNTs can be used as core in a sandwich shell. The elastic properties of these reinforced foams have been obtained by Verdejo et al. [23] where the experimental procedure and results are detailed. Scanning electron microscopy of the samples revealed an open cellular structure and a homogeneous dispersion of nanofillers. Transmission electron microscopy revealed the formation of a CNT network throughout the samples. Nanofillers showed a positive effect on the compressive response of the foams even if the thermal stability of the samples was drastically affected by their presence. The first row of Table 5 gives the Young modulus of the foam for different loading fractions of CNTs (the supposed Poisson ratio is $v = 0.25$). The density of the polymer matrix increased with nanofiller content, as expected, since it is denser than the matrix polymer. The increase in the foam densities was attributed to the changes observed in the cellular structure, because it cannot be completely attributed to the higher intrinsic density of the nanofillers. The second row gives the ratio between the density of the foam and the density of polymer. The Young modulus of the foam proposed in the third row is normalized by the relative density given in the second column in order to eliminate the density effect. Fig. 3 shows the mass density which grows when CNTs are embedded in the foam, but the increase of the Young modulus is however more convenient: the increment in percentage of the mass density of the foam with the percentage of loading fractions of CNTs is lower than the increment in percentage of the Young modulus of the foam, this feature is confirmed by the specific Young modulus (Young modulus of the foam normalized by the mass density of the foam), this last increases with the percentage of loading fractions of CNTs.

Table 5
Elastic properties of silicon foam (f) filled with different loading fractions (wt%) of CNTs. The subscript p indicates the polymer.

Loading fractions	E_f (MPa)	ρ_f/ρ_p (%)	E_{norm} (MPa)
wt0% CNTs	47.580	18.3	260
wt0.1% CNTs	190.876	23.8	802
wt0.5% CNTs	215.208	25.2	854
wt1% CNTs	235.375	26.9	875

1.1.4. Polymer matrix reinforced with clays

Polymer/clay nanocomposites are organic–inorganic nanocomposites with attractive hybrid physical and mechanical properties arising from synergistic effects among their components. Li et al. [26] have investigated the properties of the LBL PU–MTM (layer-by-layer (LBL)-assembled polyurethane–montmorillonite) clay nanocomposite with various volume fractions of nanofillers. Classical two-phase micro-mechanics models, such as the Mori–Tanaka (MT) model [27], fail to predict the mechanical stiffness of LBL PU–MTM nanocomposites [28,29]. One possible reason is that the classical two-phase MT model does not include the contribution of the interphases which are a finite zone of material surrounding the inclusions. From continuum mechanics point of view, the interphase is a region consisting of constrained polymer chains around nanoparticles which produces the presence of large strain gradients around the particles. In a nanocomposite, both the presence of an interphase and the existence of strain gradients simultaneously contribute to the stiffness enhancement mechanism and particle size effect. For these reasons Li et al. [26] have proposed a Strain Gradient Mori–Tanaka (SGMT) model by introducing the theory of strain gradient elasticity into the classical Mori–Tanaka composite model, details about this model can be found in [26]. The strain gradient effect and/or the interphase effect is crucial to understanding and evaluating, from a continuum mechanics modelling viewpoint, the correct stiffness

Table 6
Comparison between classical Mori–Tanaka scheme (MT) and the Strain Gradient Mori–Tanaka scheme (SGMT) for different volume fractions of clay reinforcements in a polymer matrix.

Clay (%V_f)	E_{MT} (MPa)	E_{SGMT} (MPa)	v_{MT}	v_{SGMT}
0	25.000	25.000	0.4800	0.4800
2	26.234	202.67	0.4795	0.4773
4	27.518	373.33	0.4789	0.4773
6	28.857	597.33	0.4784	0.4773
8	30.253	840.00	0.4778	0.4773
10	31.711	1120.0	0.4773	0.4773
12	33.235	1493.0	0.4768	0.4773
14	34.828	1866.7	0.4762	0.4773
16	36.497	2320.0	0.4757	0.4773
18	38.247	2986.6	0.4751	0.4773
20	40.084	3600.0	0.4746	0.4773

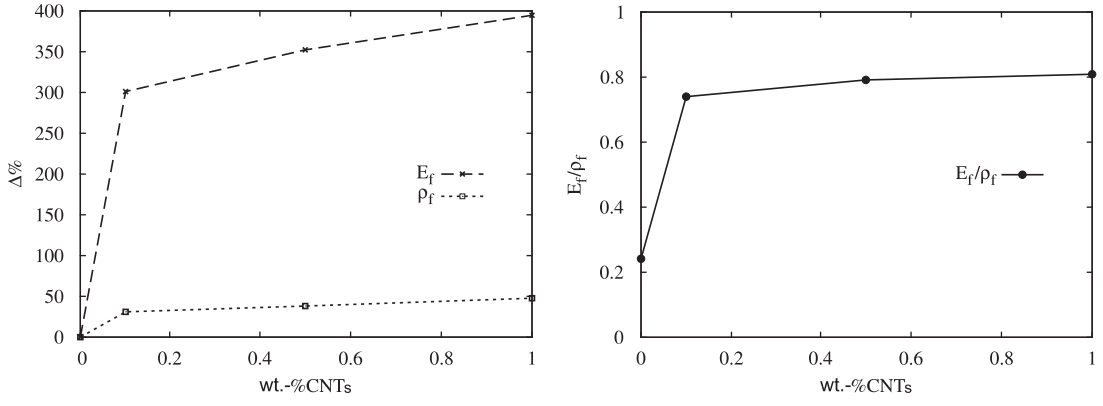

Fig. 3. Silicon foam filled with CNTs, percentage Δ% of increment of mass density and Young modulus of the foam vs. loading fractions (wt%) of CNTs (left). Specific elastic property vs. loading fractions (wt%) of CNTs (right).

enhancement efficiency of nanocomposites. Table 6 gives the graphical evaluation of the Young modulus of LBL PU–MTM nanocomposites for different volume fractions of clays proposed in [26]. The SGMT model gives completely different results from the classical MT one, and the error given by the classical MT scheme increases with the volume fraction of clay: the use of the SGMT model appears mandatory for such nanocomposites and it is very close to the experimental results given in [26]. A comparison between the Young modulus obtained via the SGMT model and its experimental values is given in Table 7 which confirms such a feature. In Fig. 4 the error made by the classical MT scheme is clearly shown and this error $\Delta\%$ increases with the volume fraction of clay. The static analysis of the shells proposed will be performed using the values of Young modulus and Poisson ratio obtained via the Strain Gradient Mori–Tanaka (SGMT) scheme, however some comparisons between the SGMT scheme and the MT one and between the SGMT model and experimental values will also be made.

2. Geometrical relations

A thin shell is a three-dimensional body bounded by two closely spaced curved surfaces, the distance between the two surfaces is small if compared with the other dimensions [30]. The middle surface of the shell is the locus of points which lie midway between these surfaces. The distance between the surfaces measured along the normal to the middle surface is the thickness of the shell at that point. Fig. 5 gives details about the geometry and the reference system of a cylindrical shell panel. The square of an infinitesimal linear segment in the layer, the associated infinitesimal area and volume are

$$ds_k^2 = H_\alpha^{k^2}\, d\alpha_k^2 + H_\beta^{k^2}\, d\beta_k^2 + H_z^{k^2}\, dz_k^2, \tag{1}$$

$$d\Omega_k = H_\alpha^k H_\beta^k\, d\alpha_k\, d\beta_k, \tag{2}$$

Table 7
Comparison between the Strain Gradient Mori–Tanaka (SGMT) scheme and experimental results for different volume fractions of clay reinforcements in a polymer matrix.

Clay ($\%V_f$)	E_{SGMT} (MPa)	E_{exper} (MPa)
5	471.43	455.88
7	711.76	764.61
9	1000.0	1000.0
12	1493.0	1676.5
20	3600.0	3600.0

$$dV_k = H_\alpha^k H_\beta^k H_z^k\, d\alpha_k\, d\beta_k\, dz_k, \tag{3}$$

where the metric coefficients, depending on the layer k and on the thickness coordinate z, are

$$H_\alpha^k = A^k(1+z_k/R_\alpha^k), \quad H_\beta^k = B^k(1+z_k/R_\beta^k), \quad H_z^k = 1. \tag{4}$$

R_α^k and R_β^k are the principal radii of curvature along the coordinates α_k and β_k, respectively. A^k and B^k are the coefficients of the first fundamental form of Ω_k (Γ_k is the Ω_k boundary). If the attention is restricted to shells with constant radii of curvature (cylindrical, spherical, toroidal geometries), the coefficients A^k and B^k equal 1. Further details for shells and their geometry are given in [30]. The geometrical relations for shells link the strains with the displacement vector. The relations split in in-plane (p) and out-of-plane (n) components are

$$\boldsymbol{\epsilon}_{pG}^k = [\epsilon_{\alpha\alpha}, \epsilon_{\beta\beta}, \gamma_{\alpha\beta}]^{kT} = (\boldsymbol{D}_p^k + \boldsymbol{A}_p^k)\, \boldsymbol{u}^k, \tag{5}$$

$$\boldsymbol{\epsilon}_{nG}^k = [\gamma_{\alpha z}, \gamma_{\beta z}, \epsilon_{zz}]^{kT} = (\boldsymbol{D}_{np}^k + \boldsymbol{D}_{nz}^k - \boldsymbol{A}_n^k)\boldsymbol{u}^k, \tag{6}$$

$\boldsymbol{\epsilon}_{pG}^k$ and $\boldsymbol{\epsilon}_{nG}^k$ are the in-plane and transverse strains, respectively. $\boldsymbol{u}^k = (u,v,w)^k$ is the displacement vector. T means the transpose

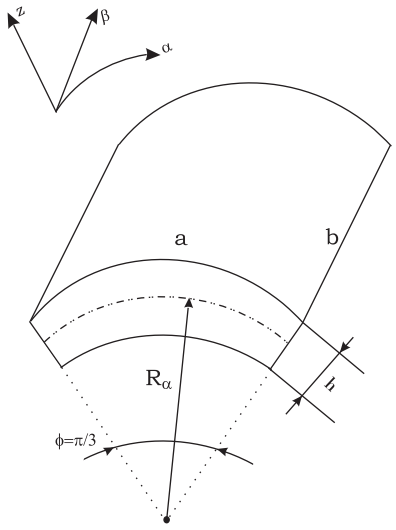

Fig. 5. Geometry and notation for the cylindrical shell panel analyzed.

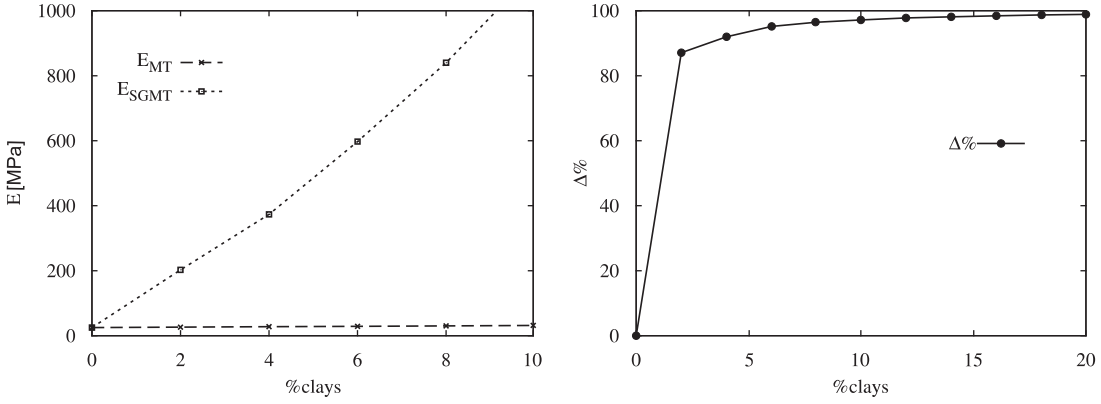

Fig. 4. Polymer matrix reinforced with clays, Young modulus obtained with the MT scheme and the SGMT scheme for different volume fractions of clays (left). Error $\Delta\% = |(E_{MT} - E_{SGMT})/E_{SGMT}| \times 100$ calculated for different volume fractions of clays (right).

of a vector. The explicit form of the introduced arrays is

$$\boldsymbol{D}_p^k = \begin{bmatrix} \frac{\partial_{\alpha_k}}{H_\alpha^k} & 0 & 0 \\ 0 & \frac{\partial_{\beta_k}}{H_\beta^k} & 0 \\ \frac{\partial_{\beta_k}}{H_\beta^k} & \frac{\partial_{\alpha_k}}{H_\alpha^k} & 0 \end{bmatrix}, \quad \boldsymbol{D}_{np}^k = \begin{bmatrix} 0 & 0 & \frac{\partial_{z_k}}{H_\alpha^k} \\ 0 & 0 & \frac{\partial_{z_k}}{H_\beta^k} \\ 0 & 0 & 0 \end{bmatrix},$$

$$\boldsymbol{D}_{nz}^k = \begin{bmatrix} \partial_{z_k} & 0 & 0 \\ 0 & \partial_{z_k} & 0 \\ 0 & 0 & \partial_{z_k} \end{bmatrix}, \tag{7}$$

$$\boldsymbol{A}_p^k = \begin{bmatrix} 0 & 0 & \frac{1}{H_\alpha^k R_\alpha^k} \\ 0 & 0 & \frac{1}{H_\beta^k R_\beta^k} \\ 0 & 0 & 0 \end{bmatrix}, \quad \boldsymbol{A}_n^k = \begin{bmatrix} \frac{1}{H_\alpha^k R_\alpha^k} & 0 & 0 \\ 0 & \frac{1}{H_\beta^k R_\beta^k} & 0 \\ 0 & 0 & 0 \end{bmatrix}. \tag{8}$$

The symbols in differential operator matrices indicate the partial derivatives $\partial_{\alpha_k} = \partial/\partial\alpha_k$, $\partial_{\beta_k} = \partial/\partial\beta_k$ and $\partial_{z_k} = \partial/\partial z_k$. The parameters H_α^k and H_β^k equal 1 in case of plates because the radii of curvature R_α^k and R_β^k are infinite, so matrices $\boldsymbol{A}_p^k$ and $\boldsymbol{A}_n^k$ are zero for plate geometries.

3. Two-dimensional shell theories

The three-dimensional problem can be reduced in a two-dimensional one in the case of shell structures [31]. Classical theories have been originally developed for one-layered isotropic shells and then extended to multilayered cases. They exhibit some difficulties for structures with higher transverse and in-plane anisotropy and moderately thickness, for these reasons the development of refined and advanced two-dimensional theories for shells is a crucial point in the structural analysis.

3.1. First order Shear Deformation Theory, FSDT

First order Shear Deformation Theory (FSDT) for multilayered structures is based on Reissner–Mindlin hypotheses [32,33]: straight lines perpendicular to the midsurface (i.e., transverse normals) before deformation remain straight after deformation and the transverse normals do not experience elongation (i.e., they are inextensible). These two assumptions imply that transverse displacement is independent of the transverse (or thickness) coordinate and the transverse normal strain ϵ_{zz} is zero. The transverse shear strains $\gamma_{\alpha z}$ and $\gamma_{\beta z}$ are included in this theory because the transverse normals do not remain perpendicular to the midsurface after deformation. The inextensibility of transverse normal allows to a constant transverse normal displacement w in the thickness direction z. The displacement model in the case of FSDT is

$$u(\alpha,\beta,z) = u_0(\alpha,\beta) + z\Phi_\alpha(\alpha,\beta),$$

$$v(\alpha,\beta,z) = v_0(\alpha,\beta) + z\Phi_\beta(\alpha,\beta),$$

$$w(\alpha,\beta,z) = w_0(\alpha,\beta). \tag{9}$$

The displacement field of FSDT has five unknowns, they are the displacements of midsurface (u_0,v_0,w_0) and the rotations (Φ_α,Φ_β). Fig. 6 indicates the typical behavior of displacement components u,v,w (linear and constant in equivalent single layer form) and transverse shear stresses $\sigma_{\alpha z},\sigma_{\beta z}$ (constant in each layer) in the thickness direction z of a multilayered shell.

3.2. Classical Lamination Theory, CLT

The Classical Lamination Theory (CLT) is the extension of Kirchhoff [34] model to multilayered structures. The additional hypothesis with respect to those given for FSDT is that the transverse normals rotate such that they remain perpendicular to the midsurface after deformation. This assumption results in zero transverse shear strains $\gamma_{\alpha z} = \gamma_{\beta z} = 0$. From the geometrical relations in Eq. (6)

$$\gamma_{\alpha z} = \frac{1}{H_\alpha^k}\frac{\partial w}{\partial \alpha_k} + \frac{\partial u}{\partial z_k} - \frac{u}{H_\alpha^k R_\alpha^k} = 0, \tag{10}$$

$$\gamma_{\beta z} = \frac{1}{H_\beta^k}\frac{\partial w}{\partial \beta_k} + \frac{\partial v}{\partial z_k} - \frac{v}{H_\beta^k R_\beta^k} = 0. \tag{11}$$

By substituting the kinematic model of Eq. (9) in Eqs. (10) and (11), it is possible to express the rotations (Φ_α and Φ_β) as functions of the other three variables u_0, v_0, and w_0. Therefore, only three degrees of freedom are used for this 2D theory, they are the displacements in the three directions referred to the midsurface. Fig. 7 shows the typical behavior of displacement components u,v,w (linear and constant in equivalent single layer form) and transverse shear stresses $\sigma_{\alpha z},\sigma_{\beta z}$ (zero for the whole multilayer) in the thickness direction z.

3.3. CUF theory

Refined models [11] are *displacements models* where higher orders of expansion in the thickness direction z are assumed for all the three displacement components. These axiomatic 2D models can be developed in Equivalent Single Layer (ESL) form when the layers embedded in the multilayer are considered as one equivalent structure, and in Layer Wise (LW) form when each layer embedded in the multilayer is separately considered in order to write the expansions in z for each k layer [31]. *Advanced mixed models* [9,10] are refined 2D models where both displacement components and transverse shear/normal stresses $\boldsymbol{\sigma}_n = (\sigma_{\alpha z},\sigma_{\beta z},\sigma_{zz})$ are "a priori" modelled. The main advantage of obtaining these stresses directly from the governing equations is the fulfillment of the Interlaminar Continuity (IC).

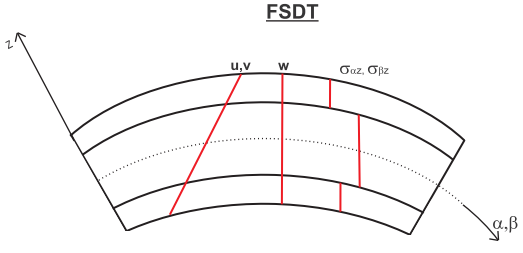

Fig. 6. FSDT for a three-layered shell: displacements and transverse shear stresses through the thickness direction z.

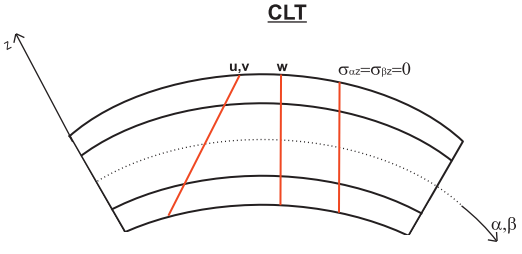

Fig. 7. CLT for a three-layered shell: displacements and transverse shear stresses through the thickness direction z.

Carrera Unified Formulation (CUF) [9–13] allows a large variety of shell models to be obtained in a unified manner. According to CUF, the 2D theories have order of expansion N which goes from first to higher order values, and depending on the used thickness functions, a model can be ESL or LW. Both refined and mixed models can be obtained. CLT and FSDT can also be obtained in the CUF framework as particular cases of the ESL theories. CLT, FSDT, ESL and LW refined and advanced mixed theories have been implemented by means of the in-house academic code MUL2 [8].

Only one CUF theory is used in this work, it is a layer wise approach where both displacement components and transverse stresses are modelled with a fourth order of expansion in the thickness direction. The z expansion for displacement components in each k layer is

$$u^k = F_0 u_0^k + F_1 u_1^k + F_2 u_2^k + F_3 u_3^k + F_4 u_4^k = F_\tau u_\tau^k,$$

$$v^k = F_0 v_0^k + F_1 v_1^k + F_2 v_2^k + F_3 v_3^k + F_4 v_4^k = F_\tau v_\tau^k,$$

$$w^k = F_0 w_0^k + F_1 w_1^k + F_2 w_2^k + F_3 w_3^k + F_4 w_4^k = F_\tau w_\tau^k, \tag{12}$$

with $\tau = 0, 1, \ldots, 4$. $k = 1, \ldots, N_l$ where N_l indicates the number of layers. 0 and 1 indicate the top (t) and bottom (b) of each layer k, respectively; $r = 2, 3, 4$ indicates the higher orders of expansion in the thickness direction. The thickness functions $F_\tau(\zeta_k)$, defined at the k-layer level, are a linear combination of Legendre polynomials $P_j = P_j(\zeta_k)$ of the jth-order in ζ_k-domain ($\zeta_k = 2z_k/h_k$ with z_k local coordinate and h_k thickness, both referred to kth layer, so $-1 \le \zeta_k \le 1$). The first five Legendre polynomials are

$$P_0 = 1, \quad P_1 = \zeta_k, \quad P_2 = \frac{(3\zeta_k^2 - 1)}{2},$$
$$P_3 = \frac{5\zeta_k^3}{2} - \frac{3\zeta_k}{2}, \quad P_4 = \frac{35\zeta_k^4}{8} - \frac{15\zeta_k^2}{4} + \frac{3}{8}, \tag{13}$$

they are combined as

$$F_t = F_0 = \frac{P_0 + P_1}{2}, \quad F_b = F_1 = \frac{P_0 - P_1}{2}, \quad F_r = P_r - P_{r-2}$$
$$\text{with } r = 2, \ldots, N. \tag{14}$$

The chosen functions have the following interesting properties:

$$\zeta_k = 1 : F_t = 1; \quad F_b = 0; \quad F_r = 0 \text{ at top}, \tag{15}$$

$$\zeta_k = -1 : F_t = 0; \quad F_b = 1; \quad F_r = 0 \text{ at bottom}. \tag{16}$$

They allow the variables to be considered as variable unknowns, and the compatibility conditions for displacements can easily be imposed at each layer interface. The LW model for transverse stresses is

$$\sigma_{\alpha z}^k = F_0 \sigma_{\alpha z 0}^k + F_1 \sigma_{\alpha z 1}^k + F_2 \sigma_{\alpha z 2}^k + F_3 \sigma_{\alpha z 3}^k + F_4 \sigma_{\alpha z 4}^k = F_\tau \sigma_{\alpha z \tau}^k,$$

$$\sigma_{\beta z}^k = F_0 \sigma_{\beta z 0}^k + F_1 \sigma_{\beta z 1}^k + F_2 \sigma_{\beta z 2}^k + F_3 \sigma_{\beta z 3}^k + F_4 \sigma_{\beta z 4}^k = F_\tau \sigma_{\beta z \tau}^k, \tag{17}$$

$$\sigma_{zz}^k = F_0 \sigma_{zz 0}^k + F_1 \sigma_{zz 1}^k + F_2 \sigma_{zz 2}^k + F_3 \sigma_{zz 3}^k + F_4 \sigma_{zz 4}^k = F_\tau \sigma_{zz \tau}^k,$$

the thickness functions $F_\tau(\zeta_k)$ have already given in Eqs. (13) and (14). The use of such thickness functions, thanks to the property remarked in Eqs. (15) and (16), allows the Interlaminar Continuity (IC) for the transverse stresses to be easily written:

$$\boldsymbol{\sigma}_{nt}^k = \boldsymbol{\sigma}_{nb}^{k+1} \quad \text{with } k = 1, \ldots, (N_l - 1), \tag{18}$$

at each interface the top value of the layer k is equal to the bottom value of the layer $(k+1)$. The same property can be used for displacements in Layer Wise form, in order to impose the compatibility conditions:

$$\boldsymbol{u}_t^k = \boldsymbol{u}_b^{k+1} \quad \text{with } k = 1, \ldots, (N_l - 1). \tag{19}$$

In Eq. (18) the vector of transverse stresses is $\boldsymbol{\sigma}_n^k = (\sigma_{\alpha z}^k, \sigma_{\beta z}^k, \sigma_{zz}^k)$. In Eq. (19) the vector of displacements is $\boldsymbol{u}^k = (u^k, v^k, w^k)$. Details about this model (in this paper it will be simply called CUF theory) can be found in [9–13]. Fig. 8 shows displacements and stresses for the CUF theory: zigzag (ZZ) form and IC are ensured for both displacement and transverse stress components. On the contrary, the transverse stresses obtained from constitutive equations could not satisfy the Interlaminar Continuity (IC) [13].

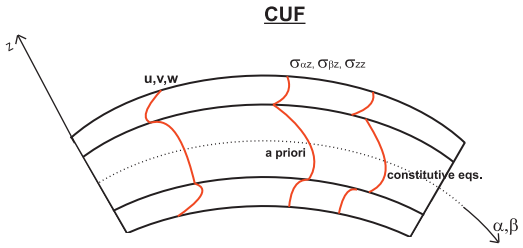

Fig. 8. CUF theory for a three-layered shell: displacements and transverse stresses through the thickness direction z.

4. Constitutive equations

Constitutive equations characterize the individual material and its reaction to applied loads. Generalized Hooke law is considered in the case of a linear constitutive model for infinitesimal deformations. These equations are written in material coordinates and then rotated in a general reference system depending by the considered problem [31]. For each k layer, the in-plane $\boldsymbol{\sigma}_p = (\sigma_{\alpha\alpha}, \sigma_{\beta\beta}, \sigma_{\alpha\beta})$ and out-plane $\boldsymbol{\sigma}_n = (\sigma_{\alpha z}, \sigma_{\beta z}, \sigma_{zz})$ stress components are linked with in-plane $\boldsymbol{\epsilon}_p = (\epsilon_{\alpha\alpha}, \epsilon_{\beta\beta}, \gamma_{\alpha\beta})$ and out-plane $\boldsymbol{\epsilon}_n = (\gamma_{\alpha z}, \gamma_{\beta z}, \epsilon_{zz})$ strain components by means of the matrix of elastic coefficients $\boldsymbol{Q}^k$ which can be split as

$$\boldsymbol{\sigma}_p^k = \boldsymbol{Q}_{pp}^k \boldsymbol{\epsilon}_p^k + \boldsymbol{Q}_{pn}^k \boldsymbol{\epsilon}_n^k, \tag{20}$$

$$\boldsymbol{\sigma}_n^k = \boldsymbol{Q}_{np}^k \boldsymbol{\epsilon}_p^k + \boldsymbol{Q}_{nn}^k \boldsymbol{\epsilon}_n^k, \tag{21}$$

where

$$\boldsymbol{Q}_{pp}^k = \begin{bmatrix} Q_{11} & Q_{12} & Q_{16} \\ Q_{12} & Q_{22} & Q_{26} \\ Q_{16} & Q_{26} & Q_{66} \end{bmatrix}^k, \quad \boldsymbol{Q}_{pn}^k = \begin{bmatrix} 0 & 0 & Q_{13} \\ 0 & 0 & Q_{23} \\ 0 & 0 & Q_{36} \end{bmatrix}^k, \tag{22}$$

$$\boldsymbol{Q}_{np}^k = \begin{bmatrix} 0 & 0 & 0 \\ 0 & 0 & 0 \\ Q_{13} & Q_{23} & Q_{36} \end{bmatrix}^k, \quad \boldsymbol{Q}_{nn}^k = \begin{bmatrix} Q_{55} & Q_{45} & 0 \\ Q_{45} & Q_{44} & 0 \\ 0 & 0 & Q_{33} \end{bmatrix}^k.$$

The meaning of coefficients Q_{ij}^k in explicit form (they depend on Young moduli, shear moduli and Poisson ratios) and their relations with coefficients in the material reference system are detailed in [31]. In the case of CLT and FSDT theories Poisson locking phenomenon appears because of the simplified kinematic assumptions in the plate/shell analysis [12,35], the assumption of zero transverse normal strain is not coherent with constitutive equations. This phenomenon is contrasted with reduced elastic coefficients which are obtained by imposing the condition $\sigma_{zz} = 0$ in Eqs. (20) and (21).

The modelled variables for advanced mixed models (CUF theory in this work) are the displacements and the transverse stresses $\boldsymbol{\sigma}_{nM}$, these last are not obtained from Eq. (21), but are "a priori" modelled (subscript M). The new constitutive equations for the mixed advanced case are obtained from Eqs. (20) and (21):

$$\boldsymbol{\sigma}_p^k = \hat{\boldsymbol{Q}}_{pp}^k \boldsymbol{\epsilon}_p^k + \hat{\boldsymbol{Q}}_{pn}^k \boldsymbol{\sigma}_{nM}^k, \tag{23}$$

$$\boldsymbol{\epsilon}_n^k = \hat{\mathbf{Q}}_{np}^k \boldsymbol{\epsilon}_p^k + \hat{\mathbf{Q}}_{nn}^k \boldsymbol{\sigma}_{nM}^k, \tag{24}$$

where the new coefficients are

$$\hat{\mathbf{Q}}_{pp}^k = \mathbf{Q}_{pp}^k - \mathbf{Q}_{pn}^k \mathbf{Q}_{nn}^{k^{-1}} \mathbf{Q}_{np}^k, \quad \hat{\mathbf{Q}}_{pn}^k = \mathbf{Q}_{pn}^k \mathbf{Q}_{nn}^{k^{-1}},$$

$$\hat{\mathbf{Q}}_{np}^k = -\mathbf{Q}_{nn}^{k^{-1}} \mathbf{Q}_{np}, \quad \hat{\mathbf{Q}}_{nn}^k = \mathbf{Q}_{nn}^{k^{-1}}. \tag{25}$$

5. Governing equations

The governing equations for the static analysis of nanocomposite shells are obtained by means of the following procedure:

- use of the appropriate variational statement, Principle of Virtual Displacements (PVD) [11] for classical theories and Reissner's Mixed Variational Theorem (RMVT) [10] for the CUF theory;
- introduction of coherent constitutive equations, Eqs. (20) and (21) for the PVD case and Eqs. (23) and (24) for the RMVT analysis;
- use of the geometrical relations for shells of Section 2;
- choice of the kinematics model for CLT, FSDT and CUF theory.

The system of governing equations for classical theories has only displacements as primary variables:

$$\boldsymbol{K}\boldsymbol{u} = \boldsymbol{p}, \tag{26}$$

$\boldsymbol{K}$ is the stiffness matrix, $\boldsymbol{u}$ is the displacement vector, $\boldsymbol{p}$ is the vector of applied loads.

In the governing equations for the CUF theory, both displacements and transverse stresses are primary variables

$$\boldsymbol{K}_{uu}\boldsymbol{u} + \boldsymbol{K}_{u\sigma}\boldsymbol{\sigma}_n = \boldsymbol{p},$$

$$\boldsymbol{K}_{\sigma u}\boldsymbol{u} + \boldsymbol{K}_{\sigma\sigma}\boldsymbol{\sigma}_n = 0, \tag{27}$$

where $\boldsymbol{\sigma}_n$ is the transverse stress vector.

Both PVD and RMVT governing equations are solved as Navier-type closed form solution via substitution of harmonic expressions for the displacements and transverse stresses, and considering the following material coefficients equal to zero: $Q_{16} = Q_{26} = Q_{36} = Q_{45} = 0$. The following harmonic assumptions can be made for the displacements and stresses, these mean simply supported boundary conditions:

$$(u_\tau^k, \sigma_{\alpha z\tau}^k) = \sum_{m,n} (\hat{U}_\tau^k, \hat{\sigma}_{\alpha z\tau}^k) \cos\left(\frac{m\pi\alpha_k}{a_k}\right) \sin\left(\frac{n\pi\beta_k}{b_k}\right), \quad k = 1, N_l,$$

$$(v_\tau^k, \sigma_{\beta z\tau}^k) = \sum_{m,n} (\hat{V}_\tau^k, \hat{\sigma}_{\beta z\tau}^k) \sin\left(\frac{m\pi\alpha_k}{a_k}\right) \cos\left(\frac{n\pi\beta_k}{b_k}\right), \quad \tau = t, b, r,$$

$$(w_\tau^k, \sigma_{zz\tau}^k) = \sum_{m,n} (\hat{W}_\tau^k, \hat{\sigma}_{zz\tau}^k) \sin\left(\frac{m\pi\alpha_k}{a_k}\right) \sin\left(\frac{n\pi\beta_k}{b_k}\right), \quad r = 2, N, \tag{28}$$

where $\hat{U}_\tau^k$, $\hat{V}_\tau^k$, $\hat{W}_\tau^k$, $\hat{\sigma}_{\alpha z\tau}^k$, $\hat{\sigma}_{\beta z\tau}^k$, $\hat{\sigma}_{zz\tau}^k$ are the amplitudes. m and n are the imposed waves number, α_k and β_k are the in-plane coordinates and a and b are in-plane shell dimensions, subscript k indicates the layer. N_l is the total number of layers, t and b indicate the top and bottom of the kth layer, respectively; r indicates the higher order of expansion with maximum value equals 4.

6. Preliminary assessment

A simply supported two-layered composite curved panel, in cylindrical bending, is used as preliminary assessment for the CUF models. A mechanical load is applied at its top surface:

$$p_z(x,y) = \hat{p}_z \sin\frac{m\pi\alpha}{a}, \tag{29}$$

the amplitude is $\hat{p}_z = 1$ Pa and wave numbers in α-direction is $m = 1$. It is made of two layers with the same thickness $h_1 = h_2 = 0.5$ h, the composite properties are longitudinal Young modulus $E_L = 25 \times 10^6$ Pa, transverse Young modulus $E_T = 1 \times 10^6$ Pa, shear moduli $G_{LT} = 0.5 \times 10^6$ Pa and $G_{TT} = 0.2 \times 10^6$ Pa, and Poisson ratios $\nu_{LT} = \nu_{TT} = 0.25$. The lamination sequence is $90^\circ/0^\circ$, the geometry is that indicated in Fig. 5 where the radius of curvature in β direction is $R_\beta = \infty$, the radius of curvature in α direction is $R_\alpha = 10$ m with angle Φ equals $\pi/3$. The two dimensions of the panel are $a = (\pi/3)R_\alpha$ and $b = 1$ m. The three-dimensional exact solution was proposed by Ren [36] in terms of non-dimensional amplitudes for stresses and displacements:

$$(\overline{\sigma}_{\alpha\alpha}, \overline{\sigma}_{\beta\beta}) = \frac{(\sigma_{\alpha\alpha}, \sigma_{\beta\beta})}{\hat{p}_z \left(\frac{R_\alpha}{h}\right)^2}, \quad (\overline{\sigma}_{\alpha z}) = \frac{(\sigma_{\alpha z})}{\hat{p}_z \left(\frac{R_\alpha}{h}\right)}, \quad \overline{w} = \frac{10 E_L w}{\hat{p}_z h \left(\frac{R_\alpha}{h}\right)^4}. \tag{30}$$

A comparison between the 3D solution by Ren [36], CLT, FSDT and CUF theory is shown in Table 8 for thick ($R_\alpha/h = 10$) and thin ($R_\alpha/h = 500$) shells. The displacement is evaluated in the middle of the thickness, the in-plane stresses at the top and the transverse shear stress at $z = h/4$. For the thick shell the use of the CUF theory is mandatory to achieve the 3D results, in particular for the transverse displacement and the transverse shear stress. Classical theories, such as CLT and FSDT, work better for the thin shell but they exhibit some difficulties for the transverse shear stress, this variable is correctly calculated by means of the CUF theory where it is a primary variable of the problem. The shell considered has both transverse and in-plane anisotropy, however the CUF theory gives a 3D description for both thick and thin cases. In [11,35,37] further assessments for shells can be found which validate the CUF theories obtained with the MUL2 software. After this preliminary assessment, the CUF theory is validated and it can reliably be used for the analysis of nanocomposite shells.

Table 8
Thick and thin composite cylindrical shell panel, normalized maximum stresses and deflections for CLT, FSDT, CUF and 3D solution.

Shell model	$\overline{w}(0)$	$\overline{\sigma}_{\alpha\alpha}(h/2)$	$\overline{\sigma}_{\beta\beta}(h/2)$	$\overline{\sigma}_{\alpha z}(h/4)$
$R_\alpha/h = 10$				
3D [36]	0.493	2.245	0.0250	0.879
CLT	0.445	2.246	0.0225	–
FSDT	0.488	2.246	0.0225	0.560
CUF	0.493	2.245	0.0249	0.879
$R_\alpha/h = 500$				
3D [36]	0.399	2.153	0.0215	0.865
CLT	0.399	2.153	0.0215	–
FSDT	0.399	2.153	0.0215	0.536
CUF	0.399	2.153	0.0215	0.865

7. Results

The new proposed benchmarks consider the same simply supported shell described in Section 6 and in Fig. 5; the load is that indicated in Eq. (29) applied at the top of the shell with amplitude $\hat{p}_z = 1$ Pa and wave numbers $m = 1$ and $n = 0$. Two thickness ratios are investigated for each case, a thick shell ($R_\alpha/h = 10$) with total thickness $h = 1$ m and a moderately thin shell ($R_\alpha/h = 500$) with total thickness $h = 0.02$ m.

7.1. Case 1: one-layered shell made of thermoplastic or elastomeric polymer reinforced with CNTs

In Table 9 the static analysis of one-layered thermoplastic shells with CNT reinforcements (both thick and thin cases) is considered. The elastic properties of the layer embedded have been given in Table 1 with constant Poisson ratio $\nu = 0.3$. Transverse displacement w and transverse shear stress $\sigma_{\alpha z}$ are evaluated in the middle of the thickness, the in-plane normal stress $\sigma_{\alpha\alpha}$ is evaluated at the top of the shell; the three variables are given as maximum amplitudes in the plane. When CNTs are added, the shell is stiffer and the transverse displacement is smaller. The introduction of CNTs is beneficial if the adherence between CNTs and matrix is included, otherwise in the case of no-adherence the introduction of CNTs does not give any improvement. The introduction of rectilinear CNTs is more incisive than the introduction of sinusoidal CNTs. In this first example only single-walled CNTs (SWCNTs) have been considered, the comparison between SWCNT and DWCNT reinforcements is given in the elastomeric polymer case. The comparison is made between CLT, FSDT and CUF theory, when the shell is thin ($R_\alpha/h = 500$) the three theories give correct values of transverse displacement and in-plane stress because it is isotropic; bigger difficulties are shown for the transverse shear stress, in this case the use of CUF theory is mandatory and CLT does not provide any result because $\sigma_{\alpha z}$ is zero as hypothesis in such a model. The use of CUF theory is mandatory in the case of thick shell ($R_\alpha/h = 10$) for all the three variables even if the shell is isotropic. In Fig. 9 the transverse displacement is given through the thickness z for both thick and thin shells by using the CUF theory, the best solution is the material embedding rectilinear SWCNTs with adherence, the most convenient sinusoidal SWCNT introduction is that proposed in the case a. In all the cases considered the volume fraction of SWCNTs equals 3%.

Table 9
Case 1, thermoplastic polymer reinforced with CNTs, thick and thin one-layered shells. Displacements and stresses obtained with classical and advanced theories.

Displacements/stresses	$R_\alpha/h = 10$			$R_\alpha/h = 500$		
	CLT	FSDT	CUF	CLT	FSDT	CUF
Thermoplastic polymer						
$w(0)$ (10^{-6} m)	0.5752	0.5875	0.5885	68 648	68 648	68 648
$\sigma_{\alpha\alpha}(h/2)$ (Pa)	74.887	74.887	75.119	187 500	187 500	187 500
$\sigma_{\alpha z}(0)$ (Pa)	–	3.9342	5.8964	–	187.69	281.53
Rectilinear SWCNTs no-adherence						
$w(0)$ (10^{-6} m)	0.5775	0.5899	0.5908	68 924	68 924	68 924
$\sigma_{\alpha\alpha}(h/2)$ (Pa)	74.887	74.887	75.119	187 500	187 500	187 500
$\sigma_{\alpha z}(0)$ (Pa)	–	3.9342	5.8964	–	187.69	281.53
Rectilinear SWCNTs with adherence						
$w(0)$ (10^{-6} m)	0.0806	0.0823	0.0825	9619.9	9620.0	9620.0
$\sigma_{\alpha\alpha}(h/2)$ (Pa)	74.887	74.887	75.119	187 500	187 500	187 500
$\sigma_{\alpha z}(0)$ (Pa)	–	3.9342	5.8964	–	187.69	281.53
$a/d = 20$, $a/l = 0.173$ SWCNTs with adherence (case a)						
$w(0)$ (10^{-6} m)	0.1100	0.1123	0.1125	13 126	13 126	13 126
$\sigma_{\alpha\alpha}(h/2)$ (Pa)	74.887	74.887	75.119	187 500	187 500	187 500
$\sigma_{\alpha z}(0)$ (Pa)	–	3.9342	5.8964	–	187.69	281.53
$a/d = 10$, $a/l = 0.43$ SWCNTs with adherence (case b)						
$w(0)$ (10^{-6} m)	0.1667	0.1703	0.1706	19 898	19 898	19 898
$\sigma_{\alpha\alpha}(h/2)$ (Pa)	74.887	74.887	75.119	187 500	187 500	187 500
$\sigma_{\alpha z}(0)$ (Pa)	–	3.9342	5.8964	–	187.69	281.53
$a/d = 20$, $a/l = 0.43$ SWCNTs with adherence (case c)						
$w(0)$ (10^{-6} m)	0.3486	0.3561	0.3566	41 605	41 605	41 605
$\sigma_{\alpha\alpha}(h/2)$ (Pa)	74.887	74.887	75.119	187 500	187 500	187 500
$\sigma_{\alpha z}(0)$ (Pa)	–	3.9342	5.8964	–	187.69	281.53

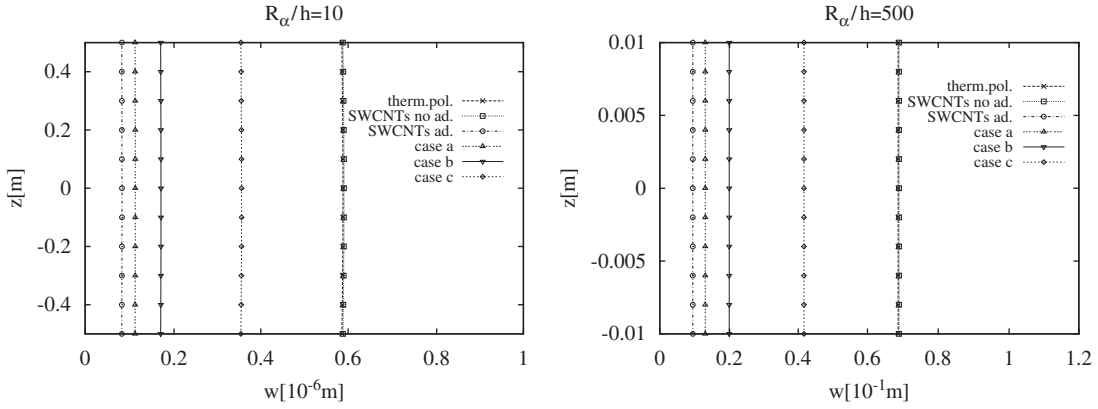

Fig. 9. Case 1, thermoplastic polymer reinforced with CNTs, thick and thin one-layered shells. Transverse displacement w vs. z by using CUF theory.

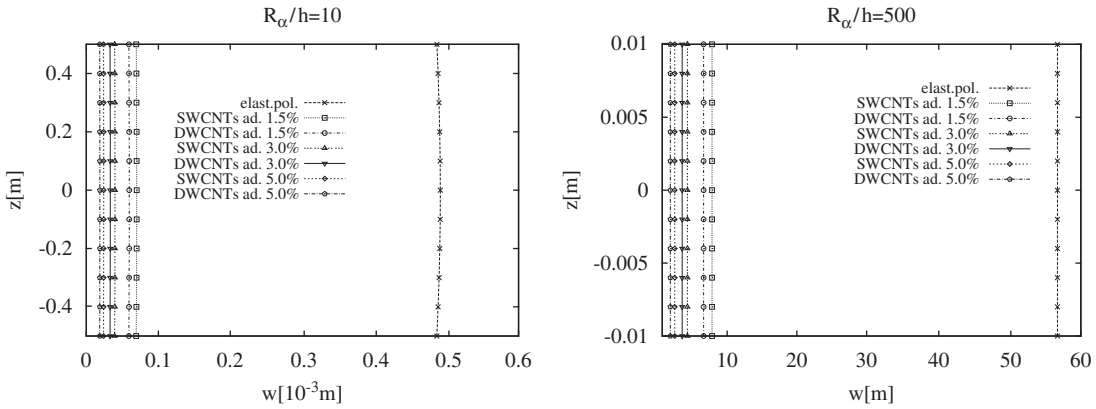

Fig. 10. Case 1, elastomeric polymer reinforced with CNTs, thick and thin one-layered shells. Transverse displacement w vs. z by using CUF theory.

The CNTs can also be embedded in an elastomeric polymer matrix, the introduction of CNT reinforcements is more effective in matrices which are less rigid (the elastomeric polymer has an initial Young modulus $E=3.11$ MPa and Poisson ration $\nu=0.499$). This fact is clearly shown in Table 2 and in Fig. 10, the difference between the case of pure elastomeric polymeric matrix and the CNT reinforced cases is bigger than the relative thermoplastic polymer case of Fig. 9. In Fig. 10 the transverse displacement is evaluated in the thickness direction z by means of CUF theory for different volume fractions of CNTs and single-walled CNTs (SWCNTs) are compared with the double-walled ones (DWCNTs), for the same volume fraction and geometry of sinusoidal CNTs the double-walled configurations are more effective than the single-walled ones. In Table 10 the same variables considered for the case of thermoplastic polymeric matrices are investigated for the elastomeric polymer case, both cases of thick and thin shells are shown. If we consider the CUF theory is clear that when the volume fraction of CNTs increases the stiffness of the shell increases too (smaller values of transverse displacements), for the same volume fraction the use of DWCNTs is better than the SWCNTs case (for the same geometry of curved CNTs). The considerations about the three proposed theories are the same already given for the thermoplastic polymer case, CLT is inadequate for the transverse shear stresses evaluation because they are zero as hypothesis in such a model. The shell is isotropic, so for thin structures CLT, FSDT and CUF theory give correct values of transverse displacement and in-plane stresses; for the thick case the use of CUF theory is mandatory to obtain a quasi-3D description of the shell in terms of displacements and stresses.

7.2. Case 2: one-layered shell made of polymer matrix embedding carbon fibers reinforced with CNTs

The shell proposed is one-layered with the polymer matrix embedding carbon fibers reinforced with CNTs. The possible geometries of the CNT inclusions are described in Fig. 2, the elastic properties of the three constituents (matrix, carbon fibers and CNTs) are given in Table 3, the elastic properties of the composite reinforced with CNTs are given in Table 4. In this benchmark the material is orthotropic with a given anisotropy, in Table 11 in-plane and transverse displacements, stresses and strains are given for both thick and thin shells in the middle of the thickness ($z=0$) or at the top ($z=h/2$). The cases compared are the fiber composite material without CNTs and the reinforcements with CNTs perpendicular to the fiber (case A) and the reinforcements with CNTs vertically positioned (case C), in both cases A and C the length of CNTs grows until to the surface of the until cell. In Table 11 it is clear how the best solution appears the case A when the transverse displacement is evaluated by using the CUF theory, CNT forest improves the transverse elastic properties of the composite. These differences are smaller in the case of thin shell ($R_\alpha/h=500$) even if the case A remains the best solution to reduce the transverse displacement. Fig. 11 shows the transverse displacement through the thickness direction z for both cases of thick and thin shells, when a thick shell is considered the best solution is the case A in order to reinforce the shell in the transverse direction, for the thin case the maximum transverse rigidity is obtained for the case D which is very close to the case A. This behavior is due to the anisotropy which leads to a thickness-dependency and suggests to use the CUF theory to capture the quasi-3D response of the shell in terms of displacements, stresses and strains. In Table 11 it is clear how for thick shells the use of CUF theory is mandatory for each considered variable, the CLT is inadequate for transverse shear stresses and strains because they are zero as hypothesis in such a theory. In the case of thin shell the use of CUF theory remains mandatory for transverse shear stresses and strains because the shell is not isotropic, the hypothesis of zero transverse stresses and strains are confirmed for the CLT.

7.3. Case 3: sandwich shell with external faces in aluminium alloy and core made of silicon foam reinforced with CNTs

This benchmark proposes a three-layered sandwich shell where the core is a silicon foam with CNT reinforcements (thickness h_2 equals 0.8 of the total thickness h) and the two external skins are in aluminium alloy *Al*2024 (thickness values of each skin h_1 and h_3 equal 0.1 of the total thickness h). The elastic properties of the reinforced foam core are given in Table 5 for different percentages of loading fractions of CNT reinforcement, the aluminium alloy is isotropic with Young modulus $E=73$ GPa and Poisson ratio $\nu=0.34$. The shell is three-layered with a given transverse anisotropy, for this reason in Table 12 the use of CUF theory appears mandatory (in particular for thick shells where the transverse displacement through the thickness is not constant as assumed in CLT and FSDT theories as hypothesis). For thick shell the errors given by CLT and FSDT are large for both transverse displacement and in-plane normal stress, these differences are smaller for the thin shell even if the correct shell description is given by the CUF theory. From the observation of Table 12, in particular in the case of thick shell, it is clear how a stiffer core, obtained with the introduction of CNTs, gives a smaller displacement and its zigzag effect decreases because the transverse anisotropy is smaller in the case of cores reinforced with CNTs.

Table 10
Case 1, elastomeric polymer reinforced with CNTs, thick and thin one-layered shells. Displacements and stresses obtained with classical and advanced theories.

Displacements/stresses	$R_\alpha/h=10$			$R_\alpha/h=500$		
	CLT	FSDT	CUF	CLT	FSDT	CUF
Elastomeric polymer						
$w(0)$ (10^{-3} m)	0.4747	0.4889	0.4884	56 653	56 654	56 654
$\sigma_{\alpha\alpha}(h/2)$ (Pa)	74.887	74.887	72.034	187 500	187 500	187 500
$\sigma_{zz}(0)$ (Pa)	–	3.9342	5.8949	–	187.69	281.53
$a/d=20$, $a/l=0.43$ SWCNTs with adherence $V_f=1.5\%$						
$w(0)$ (10^{-3} m)	0.0662	0.0682	0.0681	7898.1	7898.2	7895.8
$\sigma_{\alpha\alpha}(h/2)$ (Pa)	74.887	74.887	72.034	187 500	187 500	187 440
$\sigma_{zz}(0)$ (Pa)	–	3.9342	5.8949	–	187.69	281.45
$a/d=20$, $a/l=0.43$ DWCNTs with adherence $V_f=1.5\%$						
$w(0)$ (10^{-3} m)	0.0564	0.0581	0.0581	6736.7	6736.8	6734.4
$\sigma_{\alpha\alpha}(h/2)$ (Pa)	74.887	74.887	72.034	187 500	187 500	187 430
$\sigma_{zz}(0)$ (Pa)	–	3.9342	5.8949	–	187.69	281.43
$a/d=20$, $a/l=0.43$ SWCNTs with adherence $V_f=3.0\%$						
$w(0)$ (10^{-3} m)	0.0376	0.0388	0.0387	4491.1	4491.2	4491.6
$\sigma_{\alpha\alpha}(h/2)$ (Pa)	74.887	74.887	72.034	187 500	187 500	187 520
$\sigma_{zz}(0)$ (Pa)	–	3.9342	5.8949	–	187.69	281.56
$a/d=20$, $a/l=0.43$ DWCNTs with adherence $V_f=3.0\%$						
$w(0)$ (10^{-3} m)	0.0315	0.0324	0.0324	3754.9	3754.9	3756.5
$\sigma_{\alpha\alpha}(h/2)$ (Pa)	74.887	74.887	72.034	187 500	187 500	187 580
$\sigma_{zz}(0)$ (Pa)	–	3.9342	5.8949	–	187.69	281.65
$a/d=20$, $a/l=0.43$ SWCNTs with adherence $V_f=5.0\%$						
$w(0)$ (10^{-3} m)	0.0228	0.0235	0.0235	2726.8	2726.8	2727.9
$\sigma_{\alpha\alpha}(h/2)$ (Pa)	74.887	74.887	72.034	187 500	187 500	187 580
$\sigma_{zz}(0)$ (Pa)	–	3.9342	5.8949	–	187.69	281.64
$a/d=20$, $a/l=0.43$ DWCNTs with adherence $V_f=5.0\%$						
$w(0)$ (10^{-3} m)	0.0178	0.0183	0.0183	2120.8	2120.8	2121.3
$\sigma_{\alpha\alpha}(h/2)$ (Pa)	74.887	74.887	72.034	187 500	187 500	187 540
$\sigma_{zz}(0)$ (Pa)	–	3.9342	5.8949	–	187.69	281.60

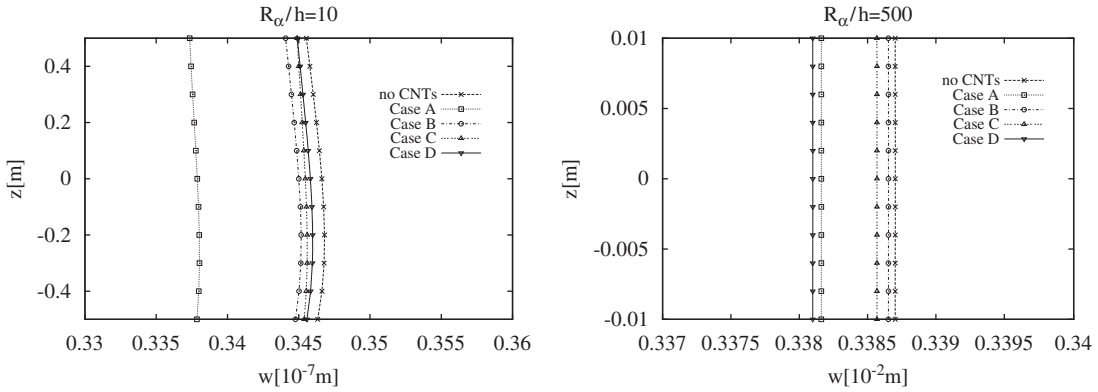

Fig. 11. Case 2, polymer matrix embedding carbon fibers with CNT reinforcement, thick and thin one-layered shells. Transverse displacement w vs. z by using CUF theory.

CLT and FSDT are equivalent single layer models and they do not capture the zigzag effect of displacements typical of sandwich structures, this effect is smaller for thin shells ($R_\alpha/h=500$). Fig. 12 shows the transverse displacement through the thickness direction of shell by using the CUF model, both thick and thin configurations are considered. In the case of thick shell, when a silicon foam core is embedded, the zigzag form of the displacement is clearly displayed; this effect is less pronounced for the relative thin shell. For both thick and thin shells, the introduction of CNTs in the silicon foam core has a double effect, it gives a stiffer core which leads to a smaller displacement and it reduces the zigzag effect of the displacement.

7.4. Case 4: one-layered shell made of polymer matrix reinforced with clays

The last benchmark considers an one-layered shell made of a polymeric matrix reinforced with clays, the elastic properties in terms of Young modulus and Poisson ratio are given in Table 6 where both Mori–Tanaka (MT) and Strain Gradient Mori–Tanaka (SGMT) schemes are used to predict them. The polymer matrix has Young modulus $E=25$ MPa and Poisson ratio $\nu=0.48$, when the volume fraction of clays increases the error made by the MT scheme increases too. The SGMT model is also very close to experimental results as shown in Table 7 and as already

Table 11
Case 2, polymer matrix embedding carbon fibers with CNT reinforcement, thick and thin one-layered shells. Displacements, stresses and strains obtained with classical and advanced theories.

Displacements/stresses/strains	$R_\alpha/h=10$			$R_\alpha/h=500$		
	CLT	FSDT	CUF	CLT	FSDT	CUF
No CNTs						
$u(h/2)$ (10^{-7} m)	0.0567	0.0741	0.0761	11 199	11 200	11 200
$w(0)$ (10^{-7} m)	0.2838	0.3357	0.3466	33 867	33 870	33 870
$\sigma_{\alpha\alpha}(h/2)$ (Pa)	74.887	74.887	77.631	187 500	187 500	187 500
$\sigma_{\alpha z}(0)$ (Pa)	–	3.9342	5.8687	–	187.69	281.53
$\epsilon_{\alpha\alpha}(h/2)$ (10^{-8})	0.1081	0.1081	0.1116	270.67	270.67	270.67
$\gamma_{\alpha z}(0)$ (10^{-8})	–	0.1385	0.2066	–	6.6087	9.9130
Case A						
$u(h/2)$ (10^{-7} m)	0.0567	0.0717	0.0761	11 181	11 182	11 182
$w(0)$ (10^{-7} m)	0.2833	0.3284	0.3379	33 813	33 816	33 816
$\sigma_{\alpha\alpha}(h/2)$ (Pa)	74.887	74.887	77.283	187 500	187 500	187 500
$\sigma_{\alpha z}(0)$ (Pa)	–	3.9342	5.8729	–	187.69	281.53
$\epsilon_{\alpha\alpha}(h/2)$ (10^{-8})	0.1079	0.1079	0.1112	270.24	270.24	270.24
$\gamma_{\alpha z}(0)$ (10^{-8})	–	0.1203	0.1796	–	5.7397	8.6095
Case C						
$u(h/2)$ (10^{-7} m)	0.0567	0.0738	0.0758	11 194	11 195	11 195
$w(0)$ (10^{-7} m)	0.2837	0.3349	0.3455	33 854	33 856	33 857
$\sigma_{\alpha\alpha}(h/2)$ (Pa)	74.887	74.887	77.587	187 500	187 500	187 500
$\sigma_{\alpha z}(0)$ (Pa)	–	3.9342	5.8695	–	187.69	281.53
$\epsilon_{\alpha\alpha}(h/2)$ (10^{-8})	0.1081	0.1081	0.1117	270.56	270.56	270.56
$\gamma_{\alpha z}(0)$ (10^{-8})	–	0.1366	0.2038	–	6.5169	9.7754

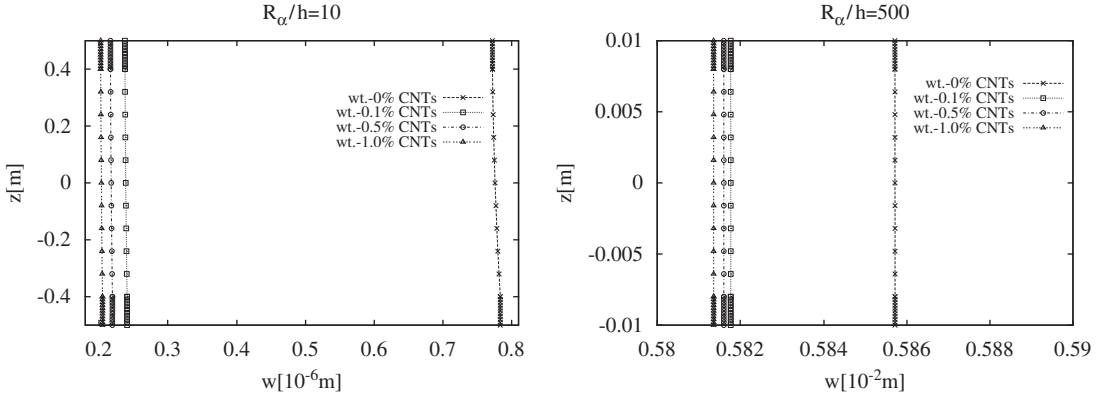

Fig. 12. Case 3, sandwich embedding a silicon foam core filled with CNTs, thick and thin shells. Transverse displacement w vs. z by using CUF theory.

demonstrated in [26]. The static analysis of the shell proposed is given in Table 13 where the elastic properties have been calculated by the SGMT scheme, the transverse displacement in the middle of the thickness and the normal in-plane stress at the top have been provided for the pure polymer matrix and for volume fractions of clays equal 4%, 8% and 16%. For thick shells the use of CLT is inadequate, FSDT gives a satisfactory analysis as the CUF theory. For thin shells the CLT works well as the other two theories because the shell is isotropic. The benefit of the introduction of clays is shown by the reduction of the transverse displacement. In Fig. 13 the transverse displacement through the thickness direction is calculated by means of the CUF theory for both thick and thin shells. In the case of pure polymer matrix no differences are shown between the MT and SGMT schemes, the differences are considerable for volume fractions of clays equal 4% and 8% and this error is independent by the thickness ratio of the shell. Table 14 shows a comparison between the transverse displacements evaluated in the middle of the shell by means of Young moduli as given in Table 7 (both SGMT and experimental values), only the CUF theory is employed for such an investigation. The evaluation of these displacements confirms the good capability of the SGMT model for the prediction of the elastic properties, a constant Poisson ratio $\nu=0.478$ has been employed for both cases.

8. Conclusions

This paper has given a complete static analysis of simply supported cylindrical shell panels made of nanocomposite layers. Different types of layered shells have been analyzed: one-layered elastomeric and thermoplastic polymer shells with CNT reinforcement, one-layered carbon fiber polymer shell with CNT reinforcement, sandwich shell with external faces in aluminum alloy and core in silicon foam filled with CNTs and one-layered polymer shell with clay reinforcement. The elastic properties of these nanocomposites have been obtained from an accurate review of the open literature. The use of the advanced two-dimensional CUF model is mandatory to investigate the static response of such nanocomposite shells. The use of classical two-dimensional theories, such as CLT and FSDT, could be

Table 12
Case 3, sandwich embedding a silicon foam core filled with CNTs and isotropic faces, thick and thin shells. Displacements and stresses obtained with classical and advanced theories.

Displacements/stresses	$R_\alpha/h=10$			$R_\alpha/h=500$		
	CLT	FSDT	CUF	CLT	FSDT	CUF
wt0% CNTs						
$w(h/2)$ (10^{-6} m)	0.0488	0.0516	0.7719	5820.6	5820.8	5857.1
$w(0)$ (10^{-6} m)	0.0488	0.0516	0.7758	5820.6	5820.8	5857.1
$w(-h/2)$ (10^{-6} m)	0.0488	0.0516	0.7834	5820.6	5820.8	5857.1
$\sigma_{zz}(h/2)$ (Pa)	153.62	153.62	363.29	383 970	383 970	384 230
wt0.1% CNTs						
$w(h/2)$ (10^{-6} m)	0.0488	0.0514	0.2377	5809.4	5809.5	5817.7
$w(0)$ (10^{-6} m)	0.0488	0.0514	0.2389	5809.4	5809.5	5817.7
$w(-h/2)$ (10^{-6} m)	0.0488	0.0514	0.2408	5809.4	5809.5	5817.7
$\sigma_{zz}(h/2)$ (Pa)	153.32	153.32	208.74	383 230	383 230	383 310
wt0.5% CNTs						
$w(h/2)$ (10^{-6} m)	0.0487	0.0514	0.2166	5807.5	5807.6	5816.0
$w(0)$ (10^{-6} m)	0.0487	0.0514	0.2177	5807.5	5807.6	5816.0
$w(-h/2)$ (10^{-6} m)	0.0487	0.0514	0.2194	5807.5	5807.6	5816.0
$\sigma_{zz}(h/2)$ (Pa)	153.27	153.27	202.60	383 100	383 100	383 270
wt1% CNTs						
$w(h/2)$ (10^{-6} m)	0.0487	0.0514	0.2024	5805.9	5806.0	5813.6
$w(0)$ (10^{-6} m)	0.0487	0.0514	0.2034	5805.9	5806.0	5813.6
$w(-h/2)$ (10^{-6} m)	0.0487	0.0514	0.2049	5805.9	5806.0	5813.6
$\sigma_{zz}(h/2)$ (Pa)	153.23	153.23	198.46	383 000	383 000	383 150

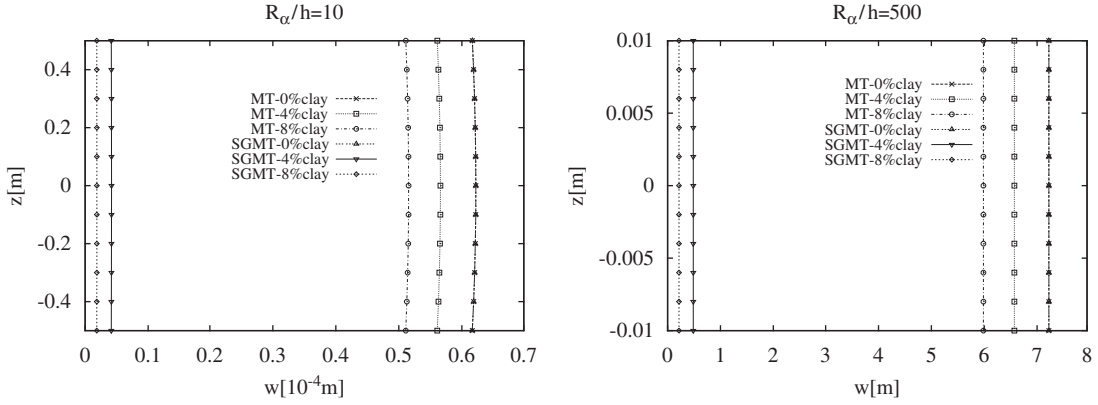

Fig. 13. Case 4, polymer matrix with clay reinforcement, thick and thin shells. Transverse displacement w vs. z by using CUF theory when the elastic properties are calculated with the Mori–Tanaka (MT) scheme or the Strain Gradient Mori–Tanaka (SGMT) scheme.

Table 13
Case 4, polymer matrix with clay reinforcement, thick and thin one-layered shells. Displacements and stresses obtained with classical and advanced theories. The elastic properties are calculated with the Strain Gradient Mori–Tanaka (SGMT) scheme.

Displacements/stresses	$R_\alpha/h=10$			$R_\alpha/h=500$		
	CLT	FSDT	CUF	CLT	FSDT	CUF
0% Clay						
$w(0)$ (10^{-4} m)	0.6051	0.6226	0.6222	72 222	72 223	72 224
$\sigma_{zz}(h/2)$ (Pa)	74.887	74.887	74.956	187 500	187 500	187 500
4% Clay						
$w(0)$ (10^{-4} m)	0.0407	0.0418	0.0417	4852.6	4852.6	4852.6
$\sigma_{zz}(h/2)$ (Pa)	74.887	74.887	74.978	187 500	187 500	187 500
8% Clay						
$w(0)$ (10^{-4} m)	0.0181	0.0186	0.0186	2156.7	2156.7	2156.7
$\sigma_{zz}(h/2)$ (Pa)	74.887	74.887	74.978	187 500	187 500	187 500
16% Clay						
$w(0)$ (10^{-5} m)	0.0654	0.0673	0.0673	7808.7	7808.8	7808.9
$\sigma_{zz}(h/2)$ (Pa)	74.887	74.887	74.978	187 500	187 500	187 500

Table 14
Case 4, polymer matrix with clay reinforcement, thick and thin one-layered shells. Displacements obtained via CUF theory. The elastic properties are calculated with the Strain Gradient Mori–Tanaka scheme (w_{SGMT}) and experimentally (w_{exper}).

% Clay	5	7	9	12	20
$R_\alpha/h = 10$					
$w_{SGMT}(0)$ (10^{-4} m)	0.0331	0.0219	0.0156	0.0104	0.0043
$w_{exper}(0)$ (10^{-4} m)	0.0342	0.0204	0.0156	0.0093	0.0043
$R_\alpha/h = 500$					
$w_{SGMT}(0)$ (10^{-4} m)	3839.5	2543.0	1810.1	1212.4	502.79
$w_{exper}(0)$ (10^{-4} m)	3970.6	2367.3	1810.1	1079.7	502.79

inappropriate for thick and moderately thick structures and/or for higher values of transverse and in-plane anisotropy. The validated advanced CUF model allows the analysis of the behavior of nanocomposite shells for different conditions: types of nanoreinforcement, their dislocation and position in the matrix, different volume fractions of fillers and several conditions at the interfaces between the nanomaterials and the matrix. The quasi-3D description of nanocomposite shells, given in the CUF model, has also allowed the quantification of the effects of nanoreinforcements in terms of displacements and stresses. The study of shell geometry does not introduce further effects, due to the curvature, with respect to the plate case already analyzed.

Acknowledgements

Financial support from the Regione Piemonte project STEPS is gratefully acknowledged.

References

[1] Lin J-C. Compression and wear behavior of composites filled with various nanoparticles. Composites: Part B 2007;38(1):79–85.
[2] Tjong SC. Structural and mechanical properties of polymer nanocomposites. Mater Sci Eng: R: Rep 2006;53(3–4):73–197.
[3] Manocha LM, Valand J, Patel N, Warrier A, Manocha S. Nanocomposites for structural applications. Indian J Pure Appl Phys 2006;44(2):135–42.
[4] Das I, Ansari SA. Nanomaterials in science and technology. J Sci Ind Res 2009;68(8):657–67.
[5] Iijima S. Helical microtubules of graphitic carbon. Nature 1991;354:56–8.
[6] Xue S, Pinnavaia TJ. Porous synthetic smectic clay for the reinforcement of epoxy polymers. Microporous Mesoporous Mater 2008;107(1–2):134–40.
[7] Brischetto S, Carrera E. Analysis of nano-reinforced layered plates via classical and refined two-dimensional theories,Multidisc Model Mater Struct, in press.
[8] MUL2. Modeling for multilayered structures in multifield analysis [online]. Available: 〈http://www.mul2.com〉 [accessed 12.10.11].
[9] Carrera E, Brischetto S, Nali P. Plates and shells for smart structures: classical and advanced theories for modeling and analysis. New Delhi, India: John Wiley and Sons Ltd.; 2011.
[10] Carrera E. Developments, ideas and evaluation based upon Reissner's mixed variational theorem in the modelling of multilayered plates and shells. Appl Mech Rev 2001;54(4):301–29.
[11] Carrera E. Theories and finite elements for multilayered plates and shells: a unified compact formulation with numerical assessment and benchmarking. Arch Comput Methods Eng 2003;10(3):215–96.
[12] Carrera E, Brischetto S. Analysis of thickness locking in classical, refined and mixed multilayered plate theories. Compos Struct 2008;82(4):549–62.
[13] Carrera E, Brischetto S. A survey with numerical assessment of classical and refined theories for the analysis of sandwich plates. Appl Mech Rev 2009;62(1):1–17.
[14] Pantano A, Capello F. Modello numerico per la caratterizzazione di materiali compositi a matrice polimerica rinforzati da nanotubi di carbonio. In: The 35th national symposium of associazione Italiana per l'analisi delle sollecitazioni (AIAS), September 13–16, 2006. Italy: Università Politecnica delle Marche; 2006.
[15] Pantano A, Boyce MC, Parks DM. Nonlinear structural mechanics based modeling of carbon nanotube deformation. Phys Rev Lett 2003;91(14):1–4.
[16] Pantano A, Parks DM, Boyce MC. Mechanics of deformation of single- and multi-wall carbon nanotubes. J Mech Phys Solids 2004;52(4):789–821.
[17] Pantano A, Boyce MC, Parks DM. Mechanics of axial compression of single and multi-wall carbon nanotubes. J Eng Mater Technol 2004;126(3):279–85.
[18] Pantano A, Parks DM, Boyce MC, Buongiorno Nardelli M. Mixed finite element-tight binding electromechanical analysis of carbon nanotubes. J Appl Phys 2004;96(11):6756–60.
[19] Frankland SJV, Caglar A, Brenner DW, Griebel M. Molecular simulation of the influence of chemical cross-links on the shear strength of carbon nanotube–polymer interfaces. J Phys Chem B 2002;106(12):3046–8.
[20] Tan P, Tong L, Sun X. Effective properties for plain weave composites through-thickness reinforced with carbon nanotube forests. Compos Struct 2008;84(1):1–10.
[21] Veedu VP, Cao A, Li X, Ma K, Soldano C, Kar S, et al. Multifunctional composites using reinforced laminae with carbon-nanotube forests. Nat Mater 2006;5(6):457–62.
[22] Thostenson ET, Li C, Chou T-W. Nanocomposites in context. Compos Sci Technol 2005;65(3–4):491–516.
[23] Verdejo R, Saiz-Arroyo C, Carretero-Gonzalez J, Barroso-Bujans F, Rodriguez-Perez MA, Lopez-Manchado MA. Physical properties of silicone foams filled with carbon nanotubes and functionalized graphene sheets. Eur Polym J 2008;44(9):2790–7.
[24] Coleman JN, Khan U, Gun'ko YK. Mechanical reinforcement of polymers using carbon nanotubes. Adv Mater 2006;18(6):689–706.
[25] Shaffer MS, Sandler J. Carbon nanotube/nanofibre polymer composites. In: Advani S, editor. World Scientific; 2006. p. 1–59.
[26] Li Y, Waas AM, Arruda EM. Strain gradient modification of the Mori–Tanaka model to predict the elastic properties of layer by layer (LBL) manufactured polymer/clay nanocomposites. In: The 51st AIAA/ASME/ASCE/AHS/ASC structures, structural dynamics, and materials conference, April 12–15, 2010. Orlando, FL, USA; 2010.
[27] Mori T, Tanaka K. Average stress in matrix and average elastic energy of materials with misfitting inclusions. Acta Metall Mater 1973;21(5):571–4.
[28] Sheng N, Boyce MC, Parks DM, Rutledge GC, Abes JI, Cohen RE. Multiscale micromechanical modeling of polymer/clay nanocomposites and the effective clay particle. Polymer 2004;45(2):487–506.
[29] Hbaieb K, Wang QX, Chia YHJ, Cotterell B. Modelling stiffness of polymer/clay nanocomposite. Polymer 2007;48(3):901–9.
[30] Leissa AW. Vibration of shells. NASA SP-288. Washington, DC, USA; 1973.
[31] Reddy JN. Mechanics of laminated composite plates and shells. Theory and analysis. Boca Raton, FL, USA: CRC Press; 2004.
[32] Reissner E. The effect of transverse shear deformation on the bending of elastic plates. J Appl Mech 1945;12(2):69–77.
[33] Mindlin RD. Influence of rotatory inertia and shear in flexural motions of isotropic elastic plates. J Appl Mech 1951;18:31–8.
[34] Kirchhoff G. Über das gleichgewicht und die bewegung einer elastishen scheibe. J Reine Angew Math 1850;40:51–88.
[35] Carrera E, Brischetto S. Analysis of thickness locking in classical, refined and mixed theories for layered shells. Compos Struct 2008;85(1):83–90.
[36] Ren JG. Exact solutions for laminated cylindrical shells in cylindrical bending. Compos Sci Technol 1987;29(3):169–87.
[37] Carrera E, Brischetto E. A comparison of various kinematic models for sandwich shell panels with soft core. J Compos Mater 2009;43(20):2201–21.